

## Chapter 5: Dynamic Force Analysis

The Carpal Wrist is a novel, parallel-architecture device with many innovative features desirable in a robotic wrist. This chapter compliments the kinematic analysis of the Carpal Wrist presented in the previous chapters by characterizing the dynamics of its parallel structure. Previous static analysis has verified the improved force bearing capacity of the Carpal Wrist, inherent in many parallel devices (Ganino, 1996). In this chapter, the parallel structure is shown to be particularly advantageous when considered dynamically, due to its light-weight structure and multiple load bearing members. The dynamic equations of motion are derived in closed-form by direct application of Lagrange's equations to the kinematic model. The model assumes a massive tool and includes all gravitational, inertial, and gyroscopic effects. The equations of motion provide closed-form evaluation of the actuation moments based on general tool trajectories.

### 5.1 Introduction to Dynamic Analysis

This chapter will perform a dynamic analysis of the Carpal Wrist. This dynamic analysis will consider the "wrist isolated" problem, one in which the Wrist dynamics are considered separate from the entire manipulator arm, and thus are derived with the base of the Wrist referenced as fixed or grounded. This approach is useful for sizing the Wrist actuators and for making comparisons between various Wrist geometries. It is also important to recognize that the Wrist-isolated problem ignores the dynamic loading that would occur on the Wrist structure due to the motion of a high-speed arm.

The results of a dynamic analysis become important when the manipulator is intended for high-speed operation or moving a massive payload resulting in measurable inertial loading. These results can provide values of the required actuator torques as well as dynamic stresses that will occur in link members. This work presents the dynamic analysis of a parallel manipulator using a Hamiltonian approach. Very few analyses of similar type are documented in archival literature. The principles demonstrated in this analysis have broad applications in the field of parallel robotics.

### 5.2 Review of Research in Manipulator Dynamics

Methods for the dynamic analysis of robotic manipulators have been studied by a number of researchers. Generalized approaches are widely available, well accepted, and are presented in robotics texts such as Craig (1989). However, these dynamic analyses are applied to serial manipulators, where every moveable element is actuated. Conversely, the dynamic analysis of parallel manipulators has been studied to a much smaller degree, in part due to their kinematic complexity. Sugimoto (1987) was one of the first researchers to present the dynamic analysis of general parallel manipulators using motor algebra. This method solves for the acceleration motor, and then gives a relation between the acceleration input vector and the acceleration motor. Using this dynamic analysis of parallel manipulators requires that equilibrium equations of all

loops in the mechanism be satisfied. For a six degree-of-freedom mechanism with six connecting chains, this requires 216 simultaneous linear equations to be solved (Sugimoto, 1989). Sugimoto also proposes a computational scheme when using motor algebra to eliminate the forces and moments acting on the passive (i.e., non-actuated) joints in a parallel structure (1989). Another approach uses the geometric influence coefficients to relate system dynamics to the state of generalized inputs (Cox and Tesar, 1990), (Sklar and Tesar, 1988). Sklar and Tesar also present a general method for the dynamic analysis of hybrid manipulator systems (systems that contain both serial and parallel modules) by deriving the influence coefficients for the general hybrid systems, thus separating the geometric parameters and the input dynamics. Geng et al., 1992, use Lagrange's equations and tensor representation for the dynamic analysis of a class of Stewart platforms. Chen derives the dynamics of a hybrid series-parallel robot using a recursive Newton-Euler formulation (1994).

Equations of motion can be generated using various approaches. Newton's Laws and Euler's Rotational Equations, D'Alembert's Principle, and Hamilton's Principle are common approaches for dynamic problems (Meirovitch, 1970, Kane, 1972). Further, the coordinate system used to describe the kinematics can be selected from either canonical forms, such as joint-space coordinates, or described using screw system kinematics.

The dynamics of the Carpal Wrist are derived using Lagrange's approach, with the generalized coordinate system chosen as the input joint angles and the kinematics developed in canonical form. The Lagrangian, expressed as a function of generalized coordinates, depends on the manipulator energy state, i.e., the potential and kinetic energy. Therefore, calculating the Lagrangian requires position and velocity information. Closed-form solutions for both the position and velocity analyses of the Carpal Wrist have been found and demonstrated in the previous chapters. Thus, the Lagrangian may be expressed in closed form. The Lagrangian formulation is advantageous since it removes internal constraint forces from the equations of motion and allows the choice of generalized coordinates, in this case the joint space coordinate system. Lagrange multipliers can be introduced as desired to inspect stress in the manipulator links due to the dynamic forces. In developing the equations of motion, tensor subscript notation will be applied throughout. The standard Einstein summation convention is assumed (Frederick and Chang, 1965). This notation will be useful as the derivatives of the velocity equations will result in third order tensors.

### 5.3 Carpal Wrist Dynamics

The Lagrangian formulation requires an analysis of the system kinetic and potential energies and tacitly assumes the system is conservative. In this analysis, the mass of the Wrist is assumed to be due entirely to the tool mass (where the tool mass includes the tool fixturing and distal plate). The mass of the leg components and midplane bearings of the wrist are assumed to be negligible relative to the mass of the tool, and are not included in the model. Since the basal plate is at the reference potential energy level and grounded it creates no inertial forces and does not become part of the Lagrangian formulation. As a result, the kinetic energy is a function of

the velocity of the tool (both translation and rotation) attached to the wrist distal plate. Likewise, the potential energy is a function of the position of the tool's center of mass.

### 5.3.1 Review of Position Information

The forward and inverse position kinematics for the Carpal Wrist are formulated in Chap. 3. The Carpal Wrist kinematic structure, shown in Fig. 5.1, consists of a base plate, which connects to the manipulator arm, and a distal plate which holds the robot's tool. The base and distal plate are connected by three symmetric five-revolute branches. Each branch consists of a base leg member and a distal leg member. The base and distal legs are connected by three intersecting revolute joints; this point of intersection is called the midplane node. The midplane nodes of the three branches form a midplane. This midplane is a plane of symmetry between the base and distal plates. The wrist is actuated by controlling the angle of the three base legs relative to the base plate, and thus controls three independent degrees of freedom of the output plane, a pointing orientation and a plunge distance along the pointing direction. A forward kinematic solution provides a functional relationship between the input joint angles, or joint space, and the output tool pose, or tool space. The forward kinematic solution begins by locating the positions of the midplane nodes given the input joint angles, and then defining the symmetric midplane. The vector normal to this symmetric midplane  $\hat{N}$  defines the pointing direction of the Wrist distal plate (the distal plate normal has twice the angular deflection of the midplane normal). Two tool space coordinates,  $\alpha$  and  $\beta$ , can therefore be defined to give the pointing direction of the distal plate as a function of the input joint angles. The third degree of freedom, plunge ( $p_d$ ) can also be found from the intersection of the midplane normal vector,  $\hat{N}$  and the base plane normal vector,  $\mathbf{z}_B$ .

The results of the position kinematics is a closed-form functional relationship between the input angles,  $\theta_i$  and the output angles,  $\alpha$  and  $\beta$ , and the plunge distance,  $p_d$ . With this functional relationship, position information can be interchangeably defined in either joint space

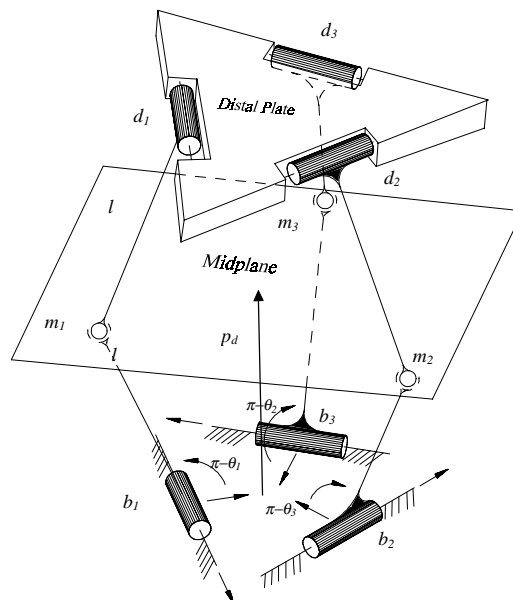


Figure 5.1: Carpal Wrist Kinematic Model

coordinates  $(\theta_1, \theta_2, \theta_3)$ , or tool space coordinates  $(\alpha, \beta, p_d)$ .

Similar to the position kinematics, a relationship between the input joint velocities and output tool velocities can be determined. The Jacobian,  $\mathbf{J}$ , related the output to input velocity components as:

$$\begin{Bmatrix} \dot{\hat{N}}_1 \\ \dot{\hat{N}}_2 \\ \dot{p} \end{Bmatrix} = J_{ij} \dot{\theta} \quad (5.1)$$

The Jacobian matrix of the Carpal Wrist was determined closed form by differentiating the position equations (Chap. 4, Canfield et al., 1996).

$$\mathbf{J} = \begin{bmatrix} \partial \hat{N}_x / \partial \theta_1 & \partial \hat{N}_x / \partial \theta_2 & \partial \hat{N}_x / \partial \theta_3 \\ \partial \hat{N}_y / \partial \theta_1 & \partial \hat{N}_y / \partial \theta_2 & \partial \hat{N}_y / \partial \theta_3 \\ \partial p_d / \partial \theta_1 & \partial p_d / \partial \theta_2 & \partial p_d / \partial \theta_3 \end{bmatrix} \quad (5.2)$$

### 5.3.2 Determining Tool Velocity

In order to write the velocity, both angular and translational, of the distal plate and attached tool with respect to the base plate, a fixed and moving coordinate frame system are assigned as shown in Fig. 5.2. A base frame,  $\{\mathbf{B}\}$  is attached to the basal plate with the  $\mathbf{z}_B$  axis normal to the base plane, and  $\mathbf{x}_B$  axis pointing toward the first base revolute joint. The base frame,  $\{\mathbf{B}\}$  is considered fixed (Newtonian) for the wrist-isolated problem. A distal frame,  $\{\mathbf{D}\}$  is attached to the Wrist output, with the  $\mathbf{z}_D$  axis normal to the distal plane (in the wrist pointing direction) and  $\mathbf{x}_D$  axis pointing toward the first distal revolute joint. Position and motion of the distal frame,  $\{\mathbf{D}\}$  describes the position and motion of the tool which is attached to the distal plate.

The position and orientation of the distal frame comes directly from the closed-form position analysis. The orientation of the distal frame relative to the base frame is a two degree of freedom specification that can be described with the two angles,  $\alpha$  and  $\beta$ , (Fig. 5.3) where  $\alpha$  and  $\beta$  are functions of the inputs,  $\theta_i$  and can be defined as:

$$\alpha = \arg(\hat{N}_1 + i\hat{N}_2) \quad (5.3)$$

$$(\frac{1}{2})\beta = \sin\left(\sqrt{\hat{N}_2^2 + \hat{N}_1^2}\right) \quad (5.4)$$

and the midplane normal vector,  $\hat{\mathbf{N}}$ , is determined from the forward or inverse kinematics. Note that both  $\alpha$  and  $\beta$  are functions of all wrist inputs,  $\theta_1$ ,  $\theta_2$ , and  $\theta_3$ .

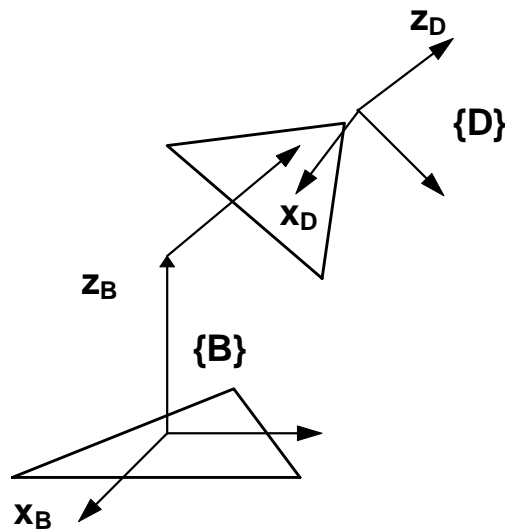


Figure 5.2: Base and Distal Frame Assignment

Angles  $\alpha$  and  $\beta$  are used to represent the pointing direction of the Wrist output, i.e., the orientation of the  $z_D$  axis. The angular change in Wrist roll, (rotation about the  $z_D$  axis) is zero, due to the kinematic constraints inherent in this parallel wrist device. Control of the tool pointing direction can be described as first a rotation of the  $\{D\}$  frame about the  $z_B$  axis by angle  $\alpha$ , and then a rotation about the rotated-intermediate frame  $y$  axis by an angle  $\beta$ . This operation is expressed in the rotation matrix,  $\mathbf{R}$  which is the matrix operator that transforms  $\{D\}$  frame coordinates into  $\{B\}$  frame coordinates.

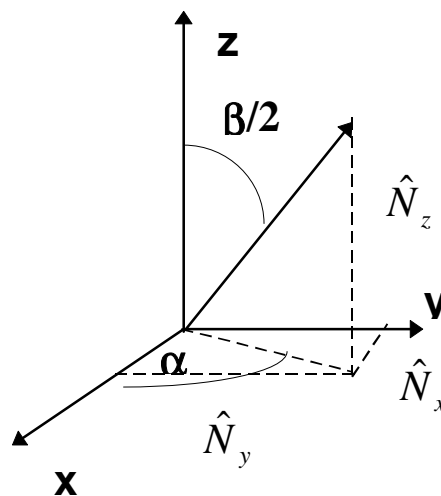


Figure 5.3 Orientation of Z axis of distal frame  $\{D\}$

$$R_{ij} = \begin{bmatrix} c\alpha c\beta & -s\alpha & c\alpha s\beta \\ s\alpha c\beta & c\alpha & s\alpha s\beta \\ -s\beta & 0 & c\beta \end{bmatrix} \quad (5.5)$$

with:

$$\begin{aligned} c\alpha &= \cos(\alpha); & s\alpha &= \sin(\alpha) \\ c\beta &= \cos(\beta); & s\beta &= \sin(\beta) \end{aligned}$$

### 5.3.2.1 Angular Velocity of the Distal Frame

Rotation of the distal frame (and the rigidly attached tool, Fig. 5.4) is caused by the time rate of change of the midplane normal,  $\hat{\mathbf{N}}$  or correspondingly the change of the orientation angles  $\alpha$  and  $\beta$ . The vector  $\omega$  will be defined as the angular velocity of the  $\{\mathbf{D}\}$  frame relative to the  $\{\mathbf{B}\}$  frame described in  $\{\mathbf{B}\}$  frame coordinates. This vector is a function of the angles  $\alpha$  and  $\beta$  and of their time rate of change.

$$\omega = f_1(\alpha, \beta, \dot{\alpha}, \dot{\beta}), \quad \omega = f_2(\theta_i, \dot{\theta}_i), \quad i = 1, 2, 3.$$

The angular velocity vector is determined from the rotation operation above as  $d\alpha/dt$  about the  $\mathbf{z}_B$  axis and then  $d\beta/dt$  about the  $y$  axis of the intermediate frame, where the intermediate frame is defined as a rotation,  $\alpha$  about the  $\mathbf{z}_B$  axis.

$$\omega_i = \begin{Bmatrix} 0 \\ 0 \\ \dot{\alpha} \end{Bmatrix} + \begin{bmatrix} c\alpha & -s\alpha & 0 \\ s\alpha & c\alpha & 0 \\ 0 & 0 & 1 \end{bmatrix} \begin{Bmatrix} 0 \\ \dot{\beta} \\ 0 \end{Bmatrix} = \begin{Bmatrix} -s\alpha\dot{\beta} \\ c\alpha\dot{\beta} \\ \dot{\alpha} \end{Bmatrix} \quad (5.6)$$

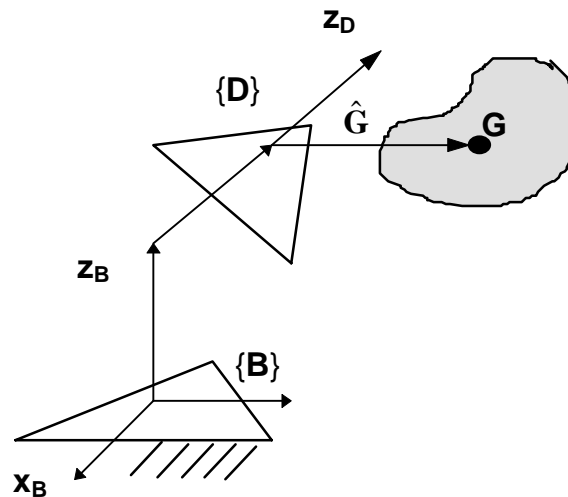


Figure 5.4: Wrist-Mounted Tool

### 5.3.2.2 Translational Velocity of the Tool Center of Mass

Referring to the frame assignment in Fig. 5.2 and mounted tool shown in Fig. 5.4,  $\mathbf{v}$  is the velocity of the tool center of mass,  $\mathbf{G}$  with respect to frame  $\{\mathbf{B}\}$  expressed in frame  $\{\mathbf{B}\}$  coordinates,

$$v_j = (\delta_{j3} + R_{j3}) J_{3k} \dot{\theta}_k + \epsilon_{jkl} \omega_k (R_{l3} p_d + R_{lm} {}^D G_m) \quad (5.7)$$

where  $\epsilon$  is the permutation tensor and  $\delta$  is the Kronecker delta. The first term in Eq. 5.7 is the linear velocity of the center of the distal frame and the second term is due to the angular velocity of the distal frame and attached tool.

### 5.3.3 Lagrange's Equations for the Wrist-Isolated Problem

Lagrange's equations are now expressed for the parallel structure Carpal Robotic Wrist.

$$\frac{d}{dt} \left( \frac{\partial \mathcal{L}}{\partial \dot{q}_i} \right) + \frac{\partial \mathcal{L}}{\partial q_i} = Q_i \quad (5.8)$$

where  $q_i$  represents the generalized coordinates and  $Q_i$  the generalized forces. The three input joint parameters are chosen as the generalized coordinates. The generalized forces associated with this choice of coordinates are the input actuator torques,  $M_i$ . Lagrange's equations become:

$$\frac{d}{dt} \left( \frac{\partial \mathcal{L}}{\partial \dot{\theta}_i} \right) - \frac{\partial \mathcal{L}}{\partial \theta_i} = M_i \quad (5.9)$$

with:

$$\mathcal{L} = T - V. \quad (5.10)$$

The kinetic and potential energies are given by:

$$\begin{aligned} T &= \frac{1}{2} m v_i v_i + \frac{1}{2} \omega_i R_{ij} I_{jk} \omega_k \\ V &= mg [p_d + R_{33} p_d + R_{3j} G_j] \end{aligned} \quad (5.11)$$

where,

$I_{jk}$  is the moment of inertia tensor of the tool expressed in the  $\{\mathbf{D}\}$  frame, and

$\mathbf{G}$  is the vector locating the tool center of mass with respect to the center of the distal plate expressed in the  $\{\mathbf{D}\}$  frame (Fig. 5.4).

#### 5.3.3.1 Derivatives of Kinetic and Potential Energy

The Lagrangian must be differentiated with respect to the inputs to the system,  $\theta_i$ , the time rate of change of these inputs,  $\dot{\theta}_i$ , and time. The necessary derivatives of both the potential and kinetic energy are:

$$\begin{aligned}\frac{\partial T}{\partial \theta_l} &= m v_i \frac{\partial v_i}{\partial \theta_l} + \frac{\partial \omega}{\partial \theta_l} R_{ij} I_{jk} \omega_k + \frac{1}{2} \omega_i \frac{\partial R_{ij}}{\partial \theta_l} I_{jk} \omega_k \\ \frac{\partial T}{\partial \dot{\theta}_l} &= m v_i \frac{\partial v_i}{\partial \dot{\theta}_l} + \frac{\partial \omega}{\partial \dot{\theta}_l} R_{ij} I_{jk} \omega_k\end{aligned}\quad (5.12)$$

$$\begin{aligned}\frac{d}{dt} \left( \frac{\partial T}{\partial \dot{\theta}_l} \right) &= m \frac{d}{dt} \left( \frac{\partial v_i}{\partial \dot{\theta}_l} \right) v_i + m \frac{\partial v_i}{\partial \dot{\theta}_l} \cdot \frac{d}{dt} (v_i) + \frac{d}{dt} \left( \frac{\partial \omega}{\partial \dot{\theta}_l} \right) R_{ij} I_{jk} \omega_k \\ &\quad + \frac{\partial \omega}{\partial \dot{\theta}_l} \frac{d}{dt} (R_{ij}) I_{jk} \omega_k + \frac{\partial \omega}{\partial \dot{\theta}_l} R_{ij} I_{jk} \frac{d}{dt} (\omega)\end{aligned}\quad (5.13)$$

$$\frac{\partial V}{\partial \theta_l} = mg \left[ \frac{\partial p_d}{\partial \theta_l} (1 + R_{33}) + p_d \frac{\partial R_{33}}{\partial \theta_l} + \frac{\partial R_{3j}}{\partial \theta_l} G_j \right]. \quad (5.14)$$

Derivatives of the energy equations require derivatives to be determined for both the angular and translational velocity. For the angular velocity vector:

$$\frac{\partial \omega}{\partial \theta_j} = \begin{Bmatrix} -s\alpha \frac{\partial \beta}{\partial \theta_j} - c\alpha \frac{\partial \alpha}{\partial \theta_j} \dot{\beta} \\ c\alpha \frac{\partial \beta}{\partial \theta_j} - s\alpha \frac{\partial \alpha}{\partial \theta_j} \dot{\beta} \\ \frac{\partial \alpha}{\partial \theta_j} \end{Bmatrix}, \quad \frac{\partial \omega}{\partial \dot{\theta}_j} = \begin{Bmatrix} -s\alpha \frac{\partial \beta}{\partial \dot{\theta}_j} \\ c\alpha \frac{\partial \beta}{\partial \dot{\theta}_j} \\ \frac{\partial \alpha}{\partial \dot{\theta}_j} \end{Bmatrix} \quad (5.15)$$

$$\frac{d\omega}{dt} = \begin{Bmatrix} -s\alpha \ddot{\beta} - c\alpha \dot{\alpha} \dot{\beta} \\ c\alpha \ddot{\beta} - s\alpha \dot{\alpha} \dot{\beta} \\ \ddot{\alpha} \end{Bmatrix} = \frac{\partial \omega}{\partial \theta_j} \dot{\theta}_j + \frac{\partial \omega}{\partial \dot{\theta}_j} \ddot{\theta}_j = \begin{Bmatrix} -s\alpha \frac{\partial \beta}{\partial \theta_j} \dot{\theta}_j - c\alpha \frac{\partial \alpha}{\partial \theta_j} \dot{\beta} \dot{\theta}_j - s\alpha \frac{\partial \beta}{\partial \dot{\theta}_j} \ddot{\theta}_j \\ c\alpha \frac{\partial \beta}{\partial \theta_j} \dot{\theta}_j - s\alpha \frac{\partial \alpha}{\partial \theta_j} \dot{\beta} \dot{\theta}_j + c\alpha \frac{\partial \beta}{\partial \dot{\theta}_j} \ddot{\theta}_j \\ \frac{\partial \alpha}{\partial \theta_j} \dot{\theta}_j + \frac{\partial \alpha}{\partial \dot{\theta}_j} \ddot{\theta}_j \end{Bmatrix} \quad (5.16)$$

$$\frac{\partial}{\partial \dot{\theta}_i} \left( \frac{\partial \omega}{\partial \dot{\theta}_j} \right) = \begin{Bmatrix} -s\alpha \frac{\partial^2 \beta}{\partial \dot{\theta}_i \partial \theta_j} - c\alpha \frac{\partial \alpha}{\partial \theta_j} \frac{\partial \beta}{\partial \dot{\theta}_i} \\ c\alpha \frac{\partial^2 \beta}{\partial \dot{\theta}_i \partial \theta_j} - s\alpha \frac{\partial \alpha}{\partial \theta_j} \frac{\partial \beta}{\partial \dot{\theta}_i} \\ \frac{\partial^2 \alpha}{\partial \dot{\theta}_i \partial \theta_j} \end{Bmatrix}. \quad (5.17)$$

The partial and time derivatives of  $\alpha$  and  $\beta$  from the equations above are functions of the midplane normal components and its derivatives.

The required derivatives of the translational velocity of the tool center of gravity,  $v$ , are:

$$\begin{aligned}\frac{\partial v}{\partial \theta_i} &= (\delta_{j3} + R_{j3}) \frac{\partial J_{3k}}{\partial \theta_i} \dot{\theta}_k + \frac{\partial R_{j3}}{\partial \theta_i} J_{3k} \dot{\theta}_k + \epsilon_{jkl} \frac{\partial \omega_k}{\partial \theta_i} R_{l3} p_d + \epsilon_{jkl} \omega_k \frac{\partial R_{l33}}{\partial \theta_i} p_d \\ &\quad + \epsilon_{jkl} \omega_k R_{l3} \frac{\partial p_d}{\partial \theta_i} + \epsilon_{jkl} \frac{\partial \omega_k}{\partial \theta_i} R_{lm} {}^D G_m + \epsilon_{jkl} \omega_k \frac{\partial R_{lm3}}{\partial \theta_i} {}^D G_m\end{aligned}\quad (5.18)$$

$$\frac{\partial v}{\partial \dot{\theta}_i} = (\delta_{j3} + R_{j3}) J_{3k} \frac{\partial \dot{\theta}_k}{\partial \dot{\theta}_i} + \epsilon_{jkl} \frac{\partial \omega_k}{\partial \dot{\theta}_i} (R_{l3} p_d + R_{lm} {}^D G_m) \quad (5.19)$$

$$\begin{aligned}\frac{dv}{dt} &= \frac{\partial R_{j3}}{\partial \theta_i} \dot{\theta}_i J_{3k} \dot{\theta}_k + (\delta_{j3} + R_{j3}) \left[ \frac{\partial J_{3k}}{\partial \theta_i} \dot{\theta}_i \dot{\theta}_k \right] + (\delta_{j3} + R_{j3}) J_{3k} \left[ \frac{\partial \dot{\theta}_k}{\partial \theta_i} \dot{\theta}_i + \frac{\partial \dot{\theta}_k}{\partial \dot{\theta}_i} \ddot{\theta}_i \right] \\ &\quad + \epsilon_{jkl} \left[ \frac{\partial \omega_k}{\partial \theta_i} \dot{\theta}_i + \frac{\partial \omega_k}{\partial \dot{\theta}_i} \ddot{\theta}_i \right] (R_{l3} p_d + R_{lm} {}^D G_m) + \epsilon_{jkl} \omega_k \left[ \frac{\partial R_{l3}}{\partial \theta_i} \dot{\theta}_i p_d + \frac{\partial R_{lm}}{\partial \theta_i} \dot{\theta}_i {}^D G_m \right]\end{aligned}\quad (5.20)$$

$$\begin{aligned}
\frac{d}{dt} \frac{\partial \gamma}{\partial \dot{\theta}_i} &= \frac{\partial R_{j3}}{\partial \theta_m} \dot{\theta}_m J_{3k} \frac{\partial \theta_k}{\partial \dot{\theta}_i} + (\delta_{j3} + R_{j3}) \left[ \frac{\partial J_{3k}}{\partial \theta_m} \dot{\theta}_m \frac{\partial \theta_k}{\partial \dot{\theta}_i} \right] + (\delta_{j3} + R_{j3}) J_{3k} \left[ \frac{\partial \theta_k}{\partial \dot{\theta}_i} \dot{\theta}_i + \frac{\partial \theta_k}{\partial \dot{\theta}_i} \ddot{\theta}_i \right] \\
&+ \epsilon_{jkl} \left[ \frac{\partial^2 \omega_k}{\partial \theta_m \partial \theta_i} \dot{\theta}_m + \frac{\partial^2 \omega_k}{\partial \theta_m \partial \theta_i} \ddot{\theta}_m \right] (R_{l3} p_d + R_{lm} {}^D G_m) \\
&+ \epsilon_{jkl} \frac{\partial \omega_k}{\partial \dot{\theta}_i} \left( \frac{\partial R_{l3}}{\partial \theta_m} \dot{\theta}_m p_d + R_{l3} \frac{\partial p_d}{\partial \theta_m} \dot{\theta}_m + \frac{\partial R_{lm}}{\partial \theta_m} \dot{\theta}_m {}^D G_m \right)
\end{aligned} \tag{5.21}$$

Derivatives of the tool space angular coordinates,  $\alpha$  and  $\beta$  are:

$$\dot{\alpha} = \frac{\hat{N}_1 \dot{\hat{N}}_2 - \hat{N}_2 \dot{\hat{N}}_1}{\hat{N}_1^2 + \hat{N}_2^2} \quad \frac{\partial \alpha}{\partial \theta_i} = \frac{\hat{N}_1 \frac{\partial \hat{N}_2}{\partial \theta_i} - \hat{N}_2 \frac{\partial \hat{N}_1}{\partial \theta_i}}{\hat{N}_1^2 + \hat{N}_2^2} \tag{5.22}$$

$$\dot{\beta} = \frac{\hat{N}_1 \dot{\hat{N}}_1 - \hat{N}_2 \dot{\hat{N}}_2}{\sqrt{1 - (\hat{N}_1^2 + \hat{N}_2^2)} \sqrt{\hat{N}_1^2 + \hat{N}_2^2}} \quad \frac{\partial \beta}{\partial \theta_i} = \frac{\hat{N}_1 \frac{\partial \hat{N}_1}{\partial \theta_i} - \hat{N}_2 \frac{\partial \hat{N}_2}{\partial \theta_i}}{\sqrt{1 - (\hat{N}_1^2 + \hat{N}_2^2)} \sqrt{\hat{N}_1^2 + \hat{N}_2^2}} \tag{5.23}$$

$$\frac{\partial \mathbf{R}}{\partial \theta_i} \begin{bmatrix} -c \alpha s \beta \frac{\partial \beta}{\partial \theta_i} - s \alpha c \beta \frac{\partial \alpha}{\partial \theta_i} & -c \alpha \frac{\partial \alpha}{\partial \theta_i} & c \alpha c \beta \frac{\partial \beta}{\partial \theta_i} - s \alpha s \beta \frac{\partial \alpha}{\partial \theta_i} \\ -s \alpha s \beta \frac{\partial \beta}{\partial \theta_i} - c \alpha c \beta \frac{\partial \alpha}{\partial \theta_i} & -s \alpha \frac{\partial \alpha}{\partial \theta_i} & s \alpha c \beta \frac{\partial \beta}{\partial \theta_i} + c \alpha s \beta \frac{\partial \alpha}{\partial \theta_i} \\ -c \beta \frac{\partial \beta}{\partial \theta_i} & 0 & -s \beta \frac{\partial \beta}{\partial \theta_i} \end{bmatrix} \tag{5.24}$$

$$\dot{\mathbf{R}} = \begin{bmatrix} -c \alpha s \beta \dot{\beta} - s \alpha c \beta \dot{\alpha} & -c \alpha \dot{\alpha} & c \alpha c \beta \dot{\beta} - s \alpha s \beta \dot{\alpha} \\ -s \alpha s \beta \frac{\partial \beta}{\partial \theta_i} - c \alpha c \beta \dot{\alpha} & -s \alpha \dot{\alpha} & s \alpha c \beta \dot{\beta} + c \alpha s \beta \dot{\alpha} \\ -c \beta \dot{\beta} & 0 & -s \beta \dot{\beta} \end{bmatrix}. \tag{5.25}$$

Finally, derivatives of the wrist Jacobian matrix,  $\mathbf{J}$ , are determined as functions of the midplane normal components and its derivatives.

### 5.3.4 Solving Lagrange's Equations

With all necessary position, velocity, and derivative terms determined, Lagrange's equations are solved for the required actuator moments,  $M_i$ ,  $i = 1, 2$ , and  $3$ . The required position, velocity, and derivative information is known from the closed-form functional relationships between the tool space and joint space coordinates. In developing the Lagrangian equations and required components, a mixture of tool-space and joint-space coordinates were used. A closed-form functional relationship between the tool-space and joint-space coordinates and their derivatives has been developed as part of the kinematic solution of this parallel device and can be expressed as:

$$(\alpha, \dot{\alpha}, \ddot{\alpha}, \beta, \dot{\beta}, \ddot{\beta}, p, \dot{p}, \ddot{p}) = g(\theta_1, \dot{\theta}_1, \ddot{\theta}_1, \theta_2, \dot{\theta}_2, \ddot{\theta}_2, \theta_3, \dot{\theta}_3, \ddot{\theta}_3).$$

Therefore, the desired tool path, which will typically be specified in tool coordinates, can be described in either tool or joint-space coordinates. With the given tool path, the required input forces are determined, solving the dynamic force analysis or forward dynamics problem. For the force-analysis problem presented, these equations are explicit algebraic equations.

## 5.4 Application to the Carpal Wrist Prototype

### Description of Experimental Dynamic Force Measurement to Verify Dynamic Model

To verify the equations of motion, a dynamic force analysis of the prototype Carpal Wrist (Appendix A) was performed using the dynamic model created above. Then the results were compared with experimental dynamic force data. A dynamic force measurement system was incorporated into the Carpal Wrist prototype carrying a generic, cylindrical-mass payload. This dynamic measurement system, shown in Fig. 5.5, recorded forces in the actuator rods that connect the stepper motors to the driven base legs of the Wrist. Axial forces in the actuator rods were measured with four strain gages, arranged in a full bridge with two longitudinal gages and two Poisson's gages, shown in detail in Fig. 5.6. The gage output was acquired and recorded through a *Metabyte DAS-16* data acquisition board. From the acquired gage voltage, force in the actuator rods was determined which could be used to calculate the input actuator moments or torques. For comparison with the analytical model, actuator rod forces were calculated from the equations of motion and compared with the actuator rod forces from the experimental model.



Figure 5.5: Dynamic Force Measurement System

The prototype performed a longitudinal move, a longitudinal slice over the hemispherical workspace sweeping from one extreme of deflection (90 deg.) to the other. The path velocity and acceleration profile were matched to the upper limit of capacity of the stepper motors driving the prototype. This move begins with a constant acceleration reaching maximum velocity in approximately 0.1875 seconds, moving across the majority of the workspace at constant velocity, and finally then decelerating in 0.1875 seconds. The time of the entire move was three seconds. A profile of the path trajectory generated for the dynamic model is shown in Fig. 5.7, while Fig. 5.8 shows the required input motor moments determined from the analytical equations of motion. Table 5.1 gives the dimensions, mass, and inertia parameters of the prototype necessary for the model. The maximum input motor moment results of Fig. 5.8 are consistent with known motor data for the prototype. The VEXTA PK264-02A stepper motors with 50:1 gear heads can produce approximately 1 Nm torque at maximum load. The model results were also compared with dynamic load data obtained experimentally. In this case, force in the actuator rods (measured in Newtons) are compared in both the analytical and experimental models. For the analytical model, this required including the kinematics of the four-bar driving transmission to obtain actuator rod force. These results are shown in Figs. 5.9 and 5.10 for the analytical and experimental results respectively. Comparing these plots demonstrates the analytical model to predict the actuator forces at approximately 30 percent smaller than actual. The trends of the profiles also show general agreement. The higher than predicted values for actuator rod force can be primarily accounted for in system friction which was not included in the model. Further, inertia forces of the leg components were considered negligible in the model causing a reduction in the predicted force. Difference in the plot profiles can be accounted for by several factors. First, the strain gage response time and averaging effects tend to integrate the force results. Additionally, the path profile given to the analytical model assumed a constant acceleration which may not have been met by the motors.

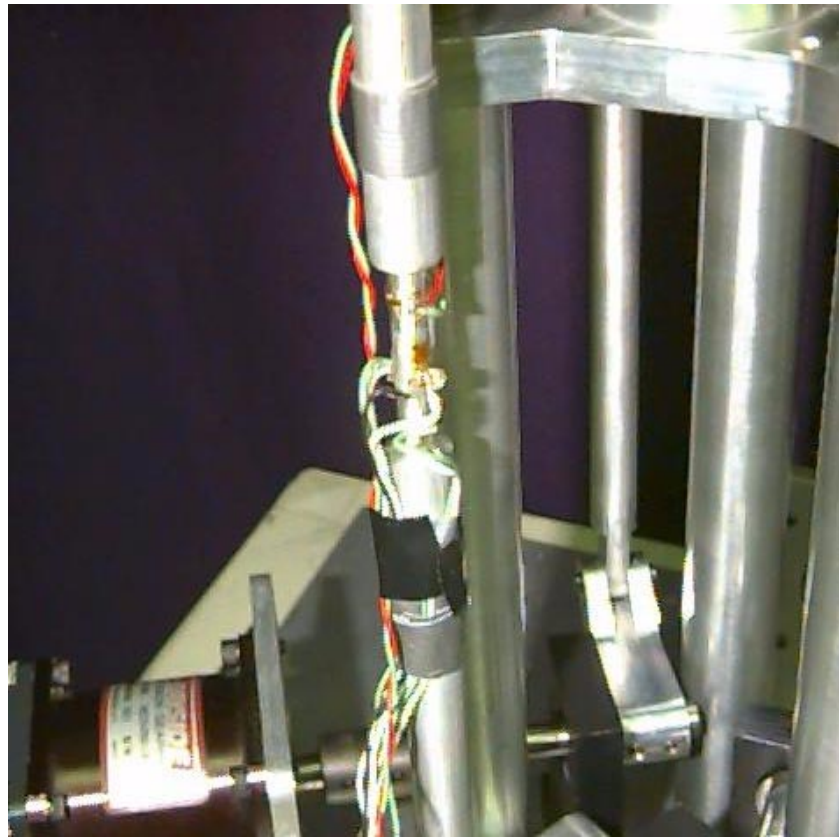


Figure 5.6: Gages on Actuating Rod

Table 5.1: Prototype Carpal Wrist Parameters for Dynamic Analysis

Element	Variable	Value
leg length	$l$	7 cm
base length	$b$	3 cm
Tool mass	$M$	1.24 kg
Tool mass moment of Inertia	$\mathbf{I}$	$\begin{bmatrix} 1.546 & 0 & 0 \\ 0 & 0.814 & 0 \\ 0 & 0 & 0.814 \end{bmatrix} \times 10^{-3} \text{kg m}^2$
Tool center of gravity	$\mathbf{G}$	2 cm

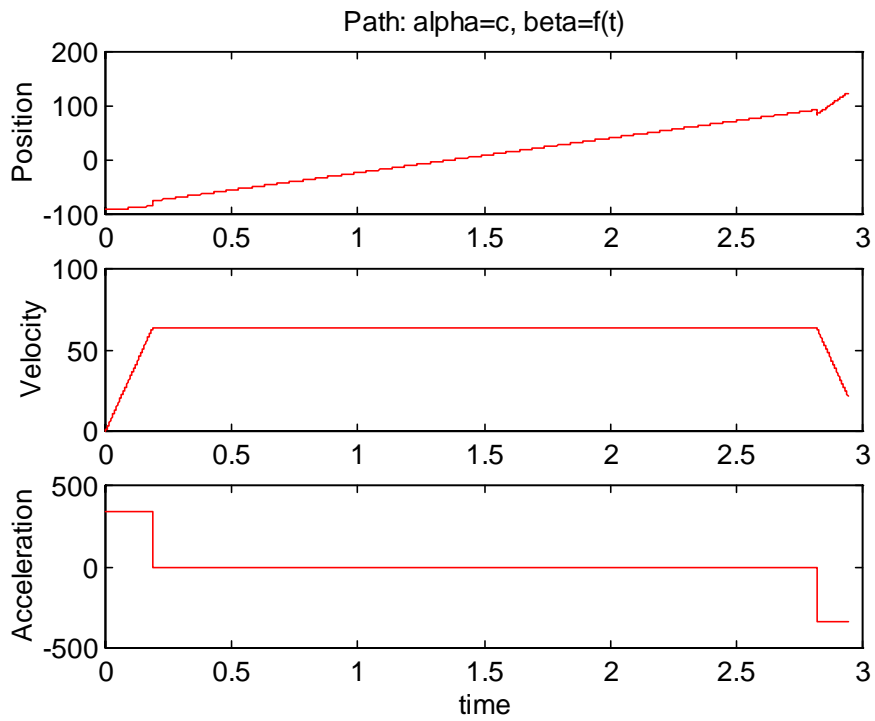


Figure 5.7: Path Trajectory for a Longitudinal Move

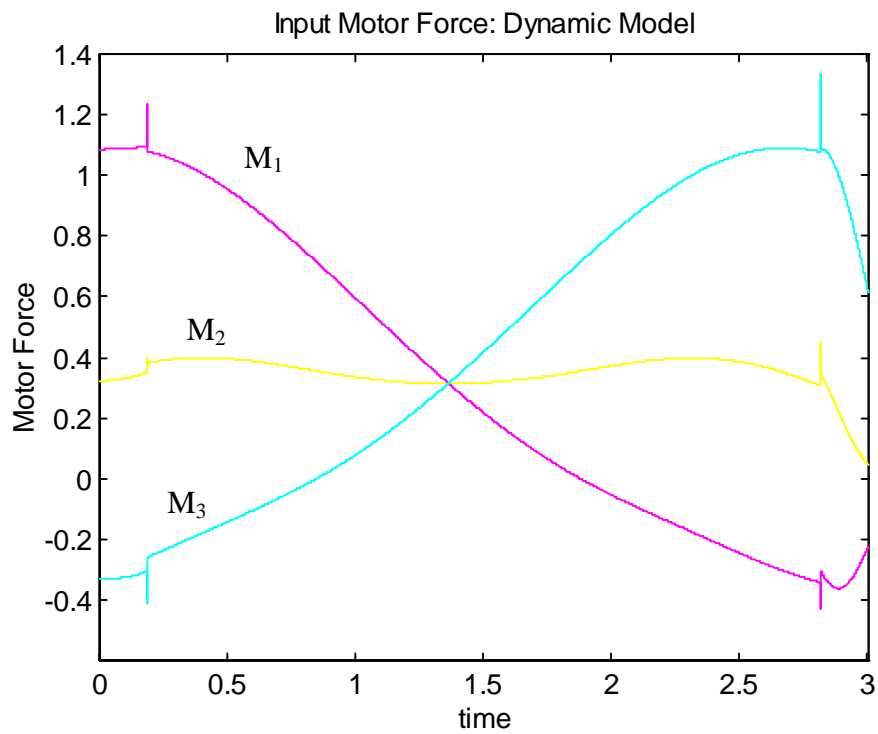


Figure 5.8: Required Motor Moment Plots: Dynamic Model

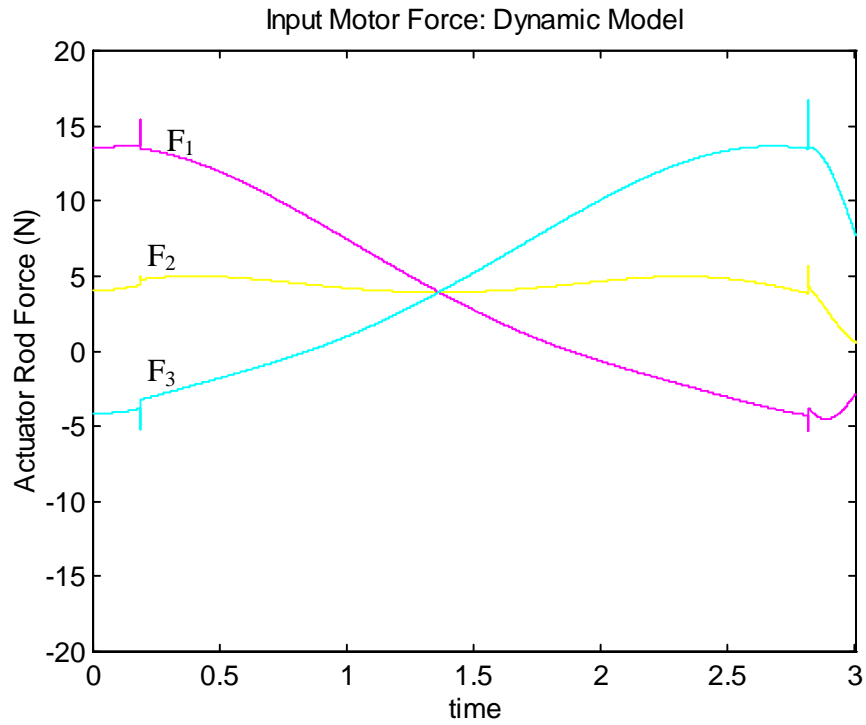


Figure 5.9: Actuator Rod Force: Dynamic Model

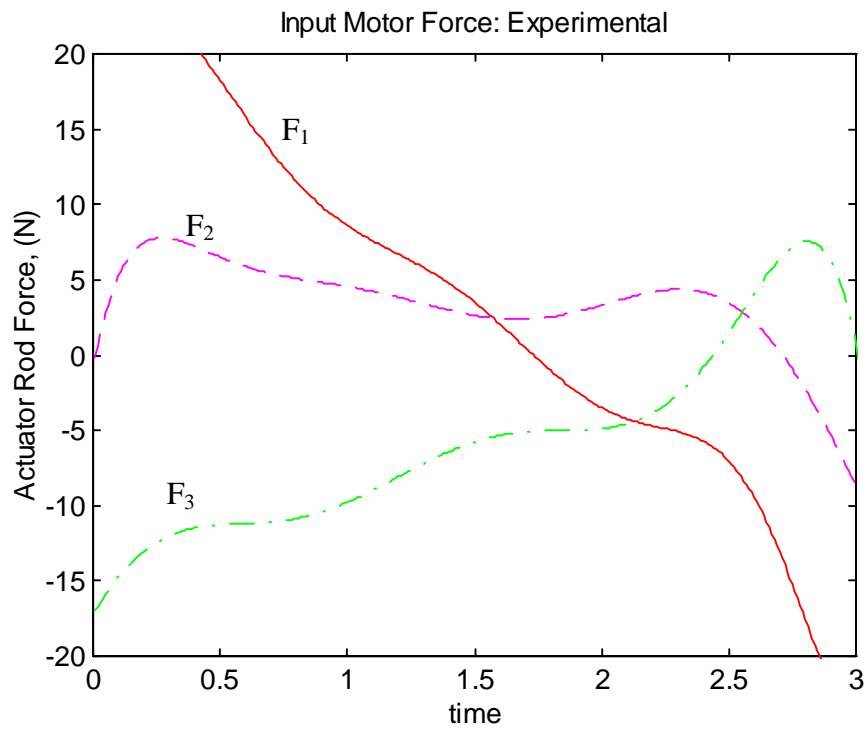


Figure 5.10: Actuator Rod Force: Experimental Model

## 5.5 Results and Conclusions

Using Hamilton's Principle, a dynamic analysis was carried out for the parallel-architecture robotic wrist. The analysis resulted in three equations of motion, determined in closed form, relating the output accelerations of the Wrist and attached tool to the input actuator moments. The process consisted of expressing the energy of the system, and then taking partial derivatives of the energy to satisfy Lagrange's Equations. One advantage of this method lies in the need for position and velocity kinematics only, which are known in closed-form for this parallel-architecture wrist. Further, the equations of motion that result from the dynamic analysis based on Hamilton's principles remove internal constraint forces and therefore result in a system of equations of number equal to the number of system inputs. In this model, the mass of the Wrist is assumed to be due entirely to the tool mass (where the tool mass includes the tool fixturing and distal plate). The mass of the leg components and midplane bearings of the wrist are assumed to be negligible relative to the mass of the tool, and are not included in the model. By ignoring this mass, an exact dynamic model is not obtained. Improvements to the dynamic model could be made by in several methods. An exact model would require a multi-body dynamic model, where the inertia of the leg components are included. The kinematic model obtained in Chaps. 3 and 4 provides the motion information necessary for such a model. A simpler improvement could be made by assuming a lumped mass body representing the legs located at an instantaneous centroid of the legs, and assuming the same instantaneous motion as the distal plate and tool.

Once the equations of motion for the Carpal Wrist were determined, they were applied to the Wrist prototype, and compared to experimental dynamic force data (Figs. 5.7-5.10). The results, while predicting lower than actual input force, verify the model. Discrepancies between the analytical and experimental model are accounted for due to friction and leg mass, both which are neglected in the analytical model.